Robust Stability Analysis of a DC/DC Buck Converter Under Multiple Parametric Uncertainties

Sharmila Sumsurooah, Milijana Odavic, *Member, IEEE*, Serhiy Bozhko, *Member, IEEE*, and Dushan Boroyevich, *Fellow, IEEE*

***Abstract*—Stability studies are a crucial part of the design of power electronic systems, especially for safety critical applications. Standard methods can guarantee stability under nominal conditions but do not take into account the multiple uncertainties that are inherent in the physical system or in the system model. These uncertainties, if unaccounted for, may lead to highly optimistic or even erroneous stability margins. The structured singular value-based μ method justifiably takes into account all possible uncertainties in the system. However, the application of the μ method to power electronic systems with multiple uncertainties is not widely discussed in the literature. This paper presents practical approaches to applying the μ method in the robust stability analysis of such uncertain systems. Further, it reveals the significant impact of various types of parametric uncertainties on the reliability of stability assessments of power electronic systems. This is achieved by examining the robust stability margin of the dc/dc buck converter system, when it is subject to variations in system load, line resistance, operating temperature, and uncertainties in the system model. The μ predictions are supported by time-domain simulation and experimental results.**

***Index Terms*—DC/DC buck power electronic (PE) converter, linear fractional transformation (LFT), robust stability analysis, structured singular value, μ analysis.**

I. Introduction

TRANSPORT accounts for nearly two-thirds of the global crude oil consumption and about a quarter of carbon dioxide emissions [1]. In order to address the issues of energy security and greenhouse emissions, a shift toward more electric-intensive architectures of transportation system, such as land vehicles, aviation, and ships, is not only needed but seems inevitable. This implies a partial to complete electrification of transport modes, which are referred to as "more electric" transport (MET) [2]. Power electronics (PE) lies at the heart of this technology transition. Yet, the susceptibility of PE systems to instability remains an important issue that needs attention [3]–[6]. Finding an answer to this problem is crucial, particularly for safety critical applications. System stability may be assessed at both the small and large signal level. Lyapunov theory of stability is generally employed to estimate large signal stability regions of the system [7]. This paper focuses on small-signal stability analysis, which is one of the important concerns in the reliable operation of the system [4], [5], [8].

While PE technology is fast evolving, the methods that are widely employed to assess the small-signal system stability are mostly based on classical techniques. These include the eigenvalue approach and impedance methods based on Nyquist stability criterion [9], [10]. Since classical methods work on the nominal model of the physical system, the outcome of the stability assessment is heavily dependent on the quality of the system model [3], [11]. The model may be refined to great detail by matching its response to that of the physical system. Yet, in practice, excessive model refinement is unlikely to be viable or practical. Further, the exact values of system components may not be known accurately. For instance, system parasitics, often hard to quantify, can have a significant influence on the quality of the model. The power supply and external filters, to be connected on site, may be unknown at the design stage. This may significantly alter the impedance of the power stage. Hence, the nominal system is bound to contain model uncertainties. From another perspective, even though a nominal model is deemed to be accurate, it may not truly represent the actual system, which is generally subject to various operating conditions uncertainties. Electrical power systems may be exposed to large variations in their loads. In aerospace applications, PE systems may be exposed to temperatures typically ranging from -40 to 125 °C [12]. In practice, PE systems may be subject to the aforementioned types of uncertainties that are normally not accounted for by classical techniques. In order to keep pace with evolving technology in PEs, there is a need to adopt new analysis techniques that duly incorporate uncertainties inherently present in the system. The structured singular value (SSV) based μ method is a robust stability analysis tool that justifiably takes into account all possible system perturbations. This paper focuses on parametric uncertainties [13], [14]. Recent works [15] and [16] demonstrate the effect of parametric uncertainties on the stability of PE-based systems.

Classical methods, which are designed for single-input-single-output systems, can include multiple uncertainties in

Manuscript received November 29, 2016; revised April 12, 2017 and June 21, 2017; accepted July 24, 2017. Date of publication August 4, 2017; date of current version February 22, 2018. Recommended for publication by Associate Editor M. Ordonez. *(Corresponding author: Sharmila Sumsurooah.)*

S. Sumsurooah and S. Bozhko are with the Department of Electrical and Electronic Engineering, The University of Nottingham, Nottingham NG7 2RD, U.K. (e-mail: sharmila.sumsurooah@nottingham.ac.uk; Serhiy.Bozhko@nottingham.ac.uk).

M. Odavic is with the Department of Electronic and Electrical Engineering, The University of Sheffield, Sheffield S10 2TN, U.K. (e-mail: M.Odavic@sheffield.ac.uk).

D. Boroyevich is with the Centre for Power Electronics Systems, Virginia Polytechnic Institute and State University, Blacksburg, VA 24061-0111 USA (e-mail: dushan@vt.edu).

Color versions of one or more of the figures in this paper are available online at http://ieeexplore.ieee.org.

Digital Object Identifier 10.1109/TPEL.2017.2736023

stability analysis. For instance, Sudhoff and Wasynczuk [17] have incorporated uncertainties in the application of the classical impedance-based energy source analysis consortium method. However, the process involves extensive parameter iteration and system linearization. In addition, the eigenvalue method is applied in combination with probabilistic stability method, such as the Monte Carlo simulation [18], [19]. However, when such classical methods are applied to multi-input multi-output (MIMO) systems, there is no guarantee that all possible combinations of uncertainties acting on the system can be evaluated to identify the most critical scenario with respect to stability [18], [20], [21]. The results may not always be reliable. Conversely, the μ method is a robust, reliable, and deterministic approach that can be employed to incorporate uncertainties in stability analysis of MIMO systems [14], [22]–[24]. Further, it does not involve a laborious iterative process. In contrast with classical techniques based on Nyquist stability criterion, the μ method provides a direct and explicit measure of the robust stability margin as a percentage of the maximum change that is allowed in an uncertain parameter for the system to remain stable. Despite the aforementioned advantages, a major drawback of the μ method is that μ cannot be computed as an exact value particularly for large size problems, since the computational burden increases exponentially with the size of the problem. A lower bound and an upper bound are calculated instead of its exact value. It has been reported in the literature that the method can be computationally expensive for the analysis of complex systems with a large number of uncertainties [25], [26]. However, a number of algorithms has been developed to reduce the gap between the μ bounds while maintaining reasonable computational time [25], [27]–[29]. Tools to optimize state-space system models and model reduction methods may be employed to decrease the computational burden [30].

Although the strength of the μ tool lies in the fact that it can be applied to system models with multiple uncertainties, the benefits of this powerful feature have been utilized or examined in a limited number of studies[21], [31]. This may be due to a few limitations that tend to make the approach hard to apply. First is the complexity of the underlying μ theory. Although a great amount of the literature is devoted to the theoretical framework, certain key aspects of the μ method are not examined from an engineering viewpoint, particularly when treating multiple uncertainties [13], [32]. Further, the methodology required to practically apply the μ tool to PE systems subject to single and multiple uncertainties is not widely discussed in the literature. In addition, the μ method is generally applied to linear systems while most systems analyzed have nonlinear behavior. A few works in the literature have successfully applied the μ method to analyze stability of conventional power systems [33]–[38]. However, the methodology applied through associated software is not discussed and multiple uncertainties are not considered. Certain works such as [25] and [39] have treated the practical aspects of the μ approach in good depth. While the results are clearly examined, the method employed are not presented in a manner that is comprehensive enough to reapply them to other systems. Other works related to the μ approach deal with μ sensitivity or the design of a robust controller as opposed to the robust stability of PE systems [18], [40]–[43].

In order to make the μ approach more application-friendly and to fully realize the benefits of the method, this paper addresses the aforementioned limitations of the μ tool. First, it presents practical approaches to apply the μ tool to a PE system subject to single and multiple uncertainties. In [44], the methodology to apply the μ tool to determine the robust stability margin of a dc/dc buck converter subject to uncertainty in load and operating temperature is presented. This paper extends the practical application of the μ tool to assess the robust stability of the aforementioned dc/dc buck converter system when it is subject to multiple uncertainties in the nominal system model. It shows how model uncertainties, which may be known to different level of accuracy, can be incorporated in robust stability analysis of the system, without compromising the reliability of the results. For the purpose of demonstrating how the μ tool supports a possible tradeoff between accuracy and simplicity in the system model, this paper evaluates the robust stability of the experimentally refined model of the system under study against that of its approximate system model. As discussed earlier, this is particularly relevant to the design engineer who, in practice, may not have sufficient information of the exact values of all system components. Second, this paper applies the modeling methodology, developed and presented in [45] and [46], to convert the nonlinear model of the dc/dc buck converter under study into an equivalent linear model that is suited for μ analysis. The modeling method is based on the symbolic linearization about an arbitrary operating point, and also caters for dependences of operating points on parameter variations. In contrast, the work in [21] does not take into account dependences of operating points on uncertainties in system parameters. In addition, this paper demonstrates the significance of the robust stability measure μ for a practical PE system subject to multiple parametric uncertainties. In [47], Sumsurooah *et al.* demonstrate the usefulness of μ by presenting the concept of the hypercube. It has been demonstrated that a system subject to N parametric uncertainties is guaranteed robustly stable within a hypercube of dimension N and of coordinate size $1/\mu$, centered about a nominal point [25], [47]. This paper applies the hypercube concept to demonstrate the significance of the μ results for the practical dc/dc buck converter system under investigation when it is subject to both single and multiple parametric uncertainties. The paper also gauges the impact of uncertainties on the reliability of stability assessments, and consequently call for the adoption of robust tools in the stability analysis of PE systems for MET applications. Experimental validation of the μ results is provided for the buck converter system under a single parametric uncertainty and then when it is exposed to an additional parametric uncertainty. Time-domain simulations are used to evaluate the μ predictions for the analyzed system when it is subject to multiple parametric uncertainties.

II. Theoretical Framework

A great advantage of the μ approach is that it works with the uncertain system model as opposed to the nominal model [14], [22]–[24]. An uncertain system model considers not only nominal values of the system parameters but also the possible range of parameter changes. In order to analyze stability of uncertain

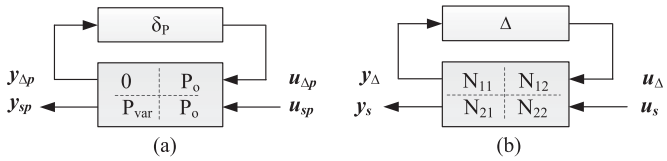

Fig. 1. (a) Uncertain parameter P as an LFT. (b) General uncertain system model $N\Delta$ as an LFT.

systems, the principle of structured singular value (μ) can be used. Prior to applying μ analysis, the system must be expressed in the linear fractional transformation (LFT) form [13], [23]. The aim is to verify that a system remains stable for all conditions that may arise within the defined uncertainty set, in which case it is said that the system is robustly stable.

LFT is a modeling technique that is employed to "pull out" the indeterminate part from the known part of a system model and place it in the feedback form. If a general uncertain parameter P is considered to be bounded in the region $[P_{\min}, P_{\max}]$, it may be represented in its normalized form δ_P bounded within $[-1, 1]$. The parameter P can be modeled as an LFT in δ_P in the expression (1) and in the matrix form in Fig. 1(a) [14], [48], where the input and output signals of the parameter are denoted as u_{sp} and y_{sp}, respectively, while $u_{\Delta p}$ and $y_{\Delta p}$ denote the output and input of δ_P [14], [39].

$$P = P_o + P_o P_{\text{var}} \delta_P, \quad \delta_P \in [-1, 1] \tag{1}$$

$$\text{where} \quad P_o = (P_{\min} + P_{\max})/2$$

$$\text{and} \quad P_{\text{var}} = \frac{(P_{\max} - P_{\min})}{2} \Big/ \frac{(P_{\max} + P_{\min})}{2}$$

The model of an entire system with parametric uncertainties can also be represented in the LFT form as shown in Fig. 1(b) and in the general LFT equation in (2) [23], [49]. The diagonal uncertainty matrix Δ as shown in Fig. 1(b) contains the set of uncertainties in their normalized form, which have been extracted from the uncertain system model.

$$F_u(N, \Delta) = \frac{y_s}{u_s} = N_{22} + N_{21}\Delta(I - N_{11}\Delta)^{-1}N_{12} \tag{2}$$

Referring to the general LFT expression (2), it can be seen that the only source that can cause the system $N\Delta$ to become unstable is the feedback term $(I - M\Delta)^{-1}$ where $M = N_{11}$ [23]. The stability of the whole system, therefore, rests on the stability of the subsystem $(I - M\Delta)^{-1}$. The robust stability condition for structured uncertainties is given by the structured singular value, as defined in

$$\mu_\Delta(M) = \frac{1}{\min[\bar{\sigma}(\Delta) : \det(I - M\Delta) = 0, \Delta \text{ structured}]} \tag{3}$$

The structured singular value, commonly denoted as μ, identifies the smallest perturbation matrix (Δ) that destabilizes the system. Thus, the SSV theory gives necessary and sufficient conditions for stability robustness [13]. For the identified smallest perturbation matrix (Δ), the system poles are at the imaginary axis [14], [22]. If μ is less than 1, the system is guaranteed to be stable for the entire uncertainty set. Further, as mentioned earlier in this paper, for a system subject to N parametric uncertainties,

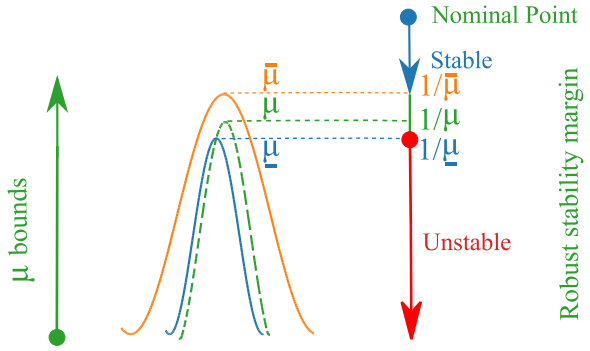

Fig. 2. Representative figure to illustrate μ bounds and robust stability margin.

μ provides the largest hypercube of dimension N, centered about the nominal point and of coordinate size $1/\mu$, within which the system can be guaranteed robustly stable. $1/\mu$ is a measure of the robust stability margin of the system [25], [45].

Since, it is generally hard to compute the exact value of μ, a lower and an upper bound to μ are calculated. The concept of the μ bounds is illustrated in Fig. 2. A lower bound $\underline{\mu}$ (which is also the upper bound of the robust stability margin) provides a sufficient condition of the instability of the system for the model perturbation $\Delta = 1/\underline{\mu}$ [25]. On the other hand, the upper bound $\bar{\mu}$ (which is also the lower bound of the robust stability margin) provides a sufficient condition that guarantees stability of the system for all perturbations that are smaller than $1/\bar{\mu}$ [25].

Although $\underline{\mu}$ is not guaranteed to be equal to μ, it is always computed at the boundary of stability [28]. Further, $\underline{\mu}$ yields the worse case perturbation model for a system [28]. On the other hand, the upper bound $\bar{\mu}$ is generally higher than μ and tends to be conservative. The worse ratio of $\mu/\bar{\mu}$ has been reported to be equal to 0.85 while in most cases the ratio is close to unity [14]. The lower bound $\underline{\mu}$ is, therefore, generally close to μ [29]. For the aforementioned reasons, the lower bound $\underline{\mu}$ is used as a good estimate of μ in this paper.

III. System Modeling for μ Analysis

The electrical network of the MET will consist of a large number of PE converters. A typical subdistribution system in the MET architecture can be represented by a source feeding power through a distribution line and an input filter to a PE interfaced load. The buck converter system, as shown in Fig. 3, has been chosen as a representation of the aforementioned subdistribution system. The general modeling method, proposed in [45] and [46], is used in this paper to convert the nonlinear buck converter system model into an equivalent linear model, which is valid for μ analysis over a range of operating points and parameter variations. The method is based on symbolic linearization around an arbitrary equilibrium point. All elements in the system model are explicitly expressed in terms of definable system parameters and input only, and for instance not in terms of indeterminate equilibrium states. The method, not being the focus in this paper, is not emphasized in this paper. The reader is referred to [45] and [46] for more details. Further, in this paper, a modular modeling approach is used in that the small-signal ac models of the power stage and the controller are built separately

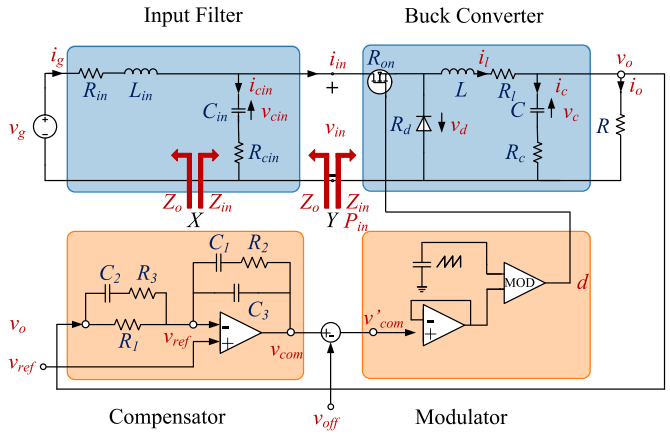

Fig. 3. Circuit representation of the closed-loop controlled buck converter with input filter.

and then combined to yield the complete linear time invariant model of the closed-loop converter, as is presented in the rest of this section [40], [50]–[52].

A. Experimental Buck Converter

The experimental closed-loop buck converter, which is used in this paper, is depicted in the circuit model in Fig. 3. The power stage is made up of an inductor–capacitor (*LC*) input filter and the open-loop buck converter [50]. The U3825 PWM controller consists of a Type III analog compensator and a modulator [53]. The sawtooth generator of the modulator generates a sawtooth waveform of peak voltage ($V_{\rm pp}$) measured as 3.52 V. The modulation gain f_m is given by $1/V_{\rm pp}$ and is equal to 0.284 [54]. The switching frequency has been measured as 51.2 kHz. The small-signal ac model of the closed-loop controlled buck converter, which is illustrated in Fig. 3, is developed in the subsequent sections. The system parameters are defined as "initial" parameters in Table I.

B. Power Stage Model

The buck converter has two operating modes over one switching period. Equations (4) and (5) describe the dynamics of the power stage when the switch is ON and OFF, respectively. The parameters in (4) and (5) are shown in Fig. 3 and described in Table I.

On-state period :

$$\frac{di_g}{dt} = (v_g - i_g R_{\rm in} - v_{\rm cin} - (i_g - i_l)R_{\rm cin})/L_{\rm in}$$
$$\frac{dv_{\rm cin}}{dt} = (i_g - i_l)/C_{\rm in}$$
$$\frac{di_l}{dt} = (v_{\rm cin} + (i_g - i_l)R_{\rm cin} - (v_o + i_l R_{\rm lon}))/L$$
$$\frac{dv_c}{dt} = (i_l - v_o/R)/C$$
$$v_o(t) = (R_c i_l + v_c)(R/(R_c + R)) \tag{4}$$

TABLE I
INITIAL AND REFINED VALUES FOR THE SYSTEM PARAMETERS

Symbol (units)	Initial values	Refined values	Description
v_g (V)	19.8	19.8	DC source voltage
$v_{\rm ref}$ (V)	5.1	5.1	Reference voltage
v_d (V)	0.22	0.22	Diode voltage
$v_{\rm off}$ (V)	2.352	2.3252	Offset voltage
f_s (kHz)	51.0	51.2	Switching frequency
f_m (−)	0.284	0.284	Modulator gain
R (Ω)	2.50	2.50	Load resistance
$R_{\rm on}$ (mΩ)	160	160	Switch-on resistance
R_d (mΩ)	12	12	Diode on-resistance
$R_{\rm in}$ (mΩ)	135	160	Input resistance
$L_{\rm in}$ μH ()	480	511.8	Input filter inductance
$C_{\rm in}$ (μF)	100	95	Input filter capacitance
$R_{\rm cin}$ (mΩ)	80	95	ESR of input filter capacitor
L (μH)	42	45.5	Output filter inductance
R_l (mΩ)	45	50	ESR of output filter inductor
C (μF)	590	540	Output filter capacitance
R_c (mΩ)	10	17	ESR of output filter capacitor
R_1 (kΩ)	20.0	19.9	Resistance in compensator
R_2 (kΩ)	20.0	19.7	Resistance in compensator
R_3 (kΩ)	2.0	2.0	Resistance in compensator
C_1 (nF)	8.22	8.22	Capacitance in compensator
C_2 (nF)	4.72	4.72	Capacitance in compensator
C_3 (nF)	0.331	0.331	Capacitance in compensator

Off-state period :

$$\frac{di_g}{dt} = (v_g - i_g R_{\rm in} - v_{\rm cin} - i_g R_{\rm cin})/L_{\rm in}$$
$$\frac{dv_{\rm cin}}{dt} = i_g/C_{\rm in}$$
$$\frac{di_l}{dt} = (-v_d - v_o - i_l R_{ld})/L$$
$$\frac{dv_c}{dt} = (i_l - v_o/R)/C$$
$$v_o(t) = (R_c i_l + v_c)(R/(R_c + R))$$
$$\text{where} \quad R_{\rm lon} = R_l + R_{\rm on}, \quad R_{ld} = R_l + R_d \tag{5}$$

The averaging modeling method is applied. Equations (4) and (5) are first represented as the state equations (6) and (7), respectively, with state vectors $x(t)$: $[i_g(t), v_{\rm cin}(t), i_l(t), v_c(t)]$, input vector $u(t)$: $[v_g(t), v_d(t)]$ and output vector $y(t)$: $[v_o(t)]$.

$$\frac{dx(t)}{dt} = A_1 x(t) + B_1 u(t), \quad y(t) = E_1 x(t) + F_1 u(t) \tag{6}$$
$$\frac{dx(t)}{dt} = A_2 x(t) + B_2 u(t), \quad y(t) = E_2 x(t) + F_2 u(t) \tag{7}$$

Then, averaging (6) and (7) over a switching period produces the system model as given by (8). This is based on the duty cycle $d(t)$ during the on-state period and $d'(t) = 1 - d(t)$ during the off-state period.

$$\frac{d\overline{x(t)}}{dt} = [d(t)A_1 + d'(t)A_2]\overline{x(t)} + [d(t)B_1 + d'(t)B_2]\overline{u(t)}$$
$$\overline{y(t)} = [d(t)E_1 + d'(t)E_2]\overline{x(t)} + [d(t)F_1 + d'(t)F_2]\overline{u(t)} \tag{8}$$

The averaged model (8) is nonlinear as it involves the multiplication of time varying quantities. In order to obtain the linear small-signal ac model of the system, the averaged model must be linearized about a dc steady-state operating point. To that end, the variables in (8) are first expanded in terms of their dc and ac components. The averaged state vector $\overline{x}(t)$, input vector $\overline{u}(t)$, output vector $\overline{y}(t)$, and duty cycle $d(t)$ are expressed in terms of their dc steady-state values X, U, Y, and D with superimposed small ac variations $\hat{x}(t)$, $\hat{u}(t)$, $\hat{y}(t)$, and $\hat{d}(t)$, respectively, as shown in (9). It can be shown that $\hat{d}(t) = -\hat{d}'(t)$.

$$\begin{aligned} \overline{x(t)} &= X + \hat{x}(t), \quad \overline{u(t)} = U + \hat{u}(t) \\ \overline{y(t)} &= Y + \hat{y}(t), \quad d(t) = D + \hat{d}(t) \end{aligned} \tag{9}$$

After substituting (9) in (8) and collecting common terms, the averaged state-space model can be written as (10) and (11).

$$\begin{aligned} &\frac{d(\hat{x}(t))}{dt} = AX + BU \\ &+ A\hat{x}(t) + B\hat{u}(t) + ((A_1 - A_2)X + (B_1 - B_2)U)\hat{d}(t) \\ &+ (A_1 - A_2)\hat{x}(t)\hat{d}(t) + (B_1 - B_2)\hat{u}(t)\hat{d}(t) \end{aligned} \tag{10}$$

$$\begin{aligned} &Y + \hat{y}(t) = EX + FU \\ &+ E\hat{x}(t) + F\hat{u}(t) + ((E_1 - E_2)X + (F_1 - F_2)U)\hat{d}(t) \\ &+ (E_1 - E_2)\hat{x}(t)\hat{d}(t) + (F_1 - F_2)\hat{u}(t)\hat{d}(t) \end{aligned} \tag{11}$$

The averaged model in steady-state corresponds to the dc terms in (10) and (11) and is given as (12).

$$\begin{aligned} 0 &= AX + BU, \quad Y = EX + FU \\ \text{where } A &= A_1 D + A_2 D', \quad B = B_1 D + B_2 D' \\ E &= E_1 D + E_2 D', \quad F = F_1 D + F_2 D' \\ D' &= 1 - D \end{aligned} \tag{12}$$

The equilibrium state can be computed as ($X = -BUA^{-1}$) with $U = [V_g, V_d]^T$ based on (12).

Symbolic linearization of the averaged model about the quiescent dc point, given by (12), involves neglecting the second-order nonlinear terms in (10) and (11) as they are very small in magnitude when compared to the linear terms. The resulting linearized small-signal ac model, in symbolic form, is obtained as (14) and (15) in its full form.

$$\begin{aligned} \frac{d\hat{i}_g(t)}{dt} &= \frac{-(R_{\text{cin}} + R_{\text{in}})}{L_{\text{in}}}\hat{i}_g(t) - \frac{1}{L_{\text{in}}}\hat{v}_{\text{cin}}(t) \\ &\quad + \frac{DR_{\text{cin}}}{L_{\text{in}}}\hat{i}_l(t) + \frac{1}{L_{\text{in}}}\hat{v}_g(t) + p_1\hat{d}(t) \\ \frac{d\hat{v}_{\text{cin}}(t)}{dt} &= \frac{1}{C_{\text{in}}}\hat{i}_g(t) - \frac{D}{C_{\text{in}}}\hat{i}_l(t) + p_2\hat{d}(t) \end{aligned}$$

$$\begin{aligned} \frac{d\hat{i}_l(t)}{dt} &= \frac{DR_{\text{cin}}}{L}\hat{i}_g(t) + \frac{D}{L}\hat{v}_{\text{cin}}(t) + \frac{q}{L}\hat{i}_l(t) \\ &\quad - \frac{R}{L(R + R_c)}\hat{v}_c(t) + \frac{D-1}{L}\hat{v}_d(t) + p_3\hat{d}(t) \\ \frac{d\hat{v}_c(t)}{dt} &= \frac{R}{C(R + R_c)}\hat{i}_l(t) - \frac{1}{C(R + R_c)}\hat{v}_c(t) \end{aligned} \tag{13}$$

$$\hat{v}_o(t) = \frac{R_c R}{R_c + R}\hat{i}_l(t) + \frac{R}{R_c + R}\hat{v}_c(t) \tag{14}$$

where

$$\begin{aligned} k_1 &= R + R_l + R_d + D^2(R_{\text{in}} - R_{\text{cin}}) \\ &\quad + D(R_{\text{cin}} - R_d + R_{\text{on}}) \\ k_2 &= \frac{RR_c}{R + Rc}, \quad k_3 = DV_g + (D-1)V_d \\ k_4 &= (R + R_l + R_d)V_g + DR_{\text{in}}V_d + DR_{\text{cin}}V_g \\ &\quad + D(R_{\text{on}} - R_d)V_g - D^2(R_{\text{cin}}V_g + R_{\text{in}}V_d) \\ p_1 &= \frac{R_{\text{cin}}k_3}{L_{\text{in}}k_1} \\ p_2 &= -\frac{k_3}{C_{\text{in}}k_1} \\ p_3 &= \frac{k_3(R_d - R_{\text{cin}} - R_{\text{on}})}{Lk_1} + \frac{k_4}{Lk_1} + \frac{DR_{\text{cin}}k_3}{Lk_1} + \frac{V_d}{L} \end{aligned}$$

C. Controller Model

The transfer functions of the compensator and modulator, shown in Fig. 3, can be written as (16) and (17), respectively.

$$\begin{aligned} G_c(s) &= \frac{v_{\text{com}}(s) - v_{\text{ref}}(s)}{v_{\text{ref}} - v_o(s)} \\ &= \frac{k(s + w_{z1})(s + w_{z2})}{s(s + w_{p2})(s + w_{p3})} \end{aligned} \tag{15}$$

$$d(s) = f_m\left(v_{\text{com}}(s) - v_{\text{off}}(s)\right) \tag{16}$$

where

$$\begin{aligned} k &= \frac{(R_1 + R_3)}{R_1 R_3 C_3} \\ w_{z1} &= \frac{1}{C_1 R_2}, \quad w_{z2} = \frac{1}{C_2(R_1 + R_3)} \\ w_{p2} &= \frac{1}{C_2 R_3}, \quad w_{p3} = \frac{(C_1 + C_3)}{C_1 C_3 R_2} \end{aligned}$$

Based on the above transfer functions, the state equations of the small-signal ac model of the controller can be obtained as (18) and (19), respectively, with state vector $\hat{x}(t)$: [$\hat{x}_5(t)$, $\hat{x}_6(t)$, $\hat{x}_7(t)$], input vector $\hat{u}(t)$: [$\hat{v}_{\text{ref}}(t), \hat{v}_{\text{off}}(t)$] and output vector $\hat{y}(t)$: [$\hat{d}(t)$].

$$\begin{aligned} \dot{\hat{x}}_5(t) &= -(w_{p2} + w_{p3})\hat{x}_5(t) - w_{p2}w_{p3}\hat{x}_6(t) \\ &\quad + \hat{v}_{\text{ref}}(t) - \hat{v}_o(t) \\ \dot{\hat{x}}_6(t) &= \hat{x}_5(t) \\ \dot{\hat{x}}_7(t) &= \hat{x}_6(t) \end{aligned} \tag{17}$$

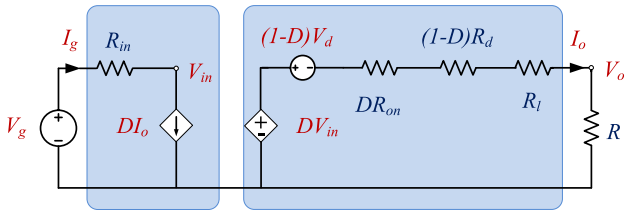

Fig. 4. Model of the buck converter in steady state.

$$\hat{d}(t) = m_1\hat{x}_5(t) + m_2\hat{x}_6(t) + m_3\hat{x}_7(t) + f_m\hat{v}_{\text{ref}}(t)) - f_m\hat{v}_{\text{off}}(t) \tag{18}$$

$$\text{where} \quad m_1 = f_m k, \quad m_2 = f_m k(w_{z1} + w_{z2}) \quad m_3 = f_m k w_{z1} w_{z2}$$

D. Closed-Loop Controlled Converter Model

At this point, the power stage and controller models, derived in the earlier sections, can be combined to yield the small-signal ac model of the closed-loop controlled buck converter. The process involves replacing $\hat{v}_o(t)$ in (18) with expression (15), and $\hat{d}(t)$ in (14) with expression (19). The resulting state-space model has state vector $\hat{x}(t) = [\hat{i}_g(t), \hat{v}_{\text{cin}}(t), \hat{i}_l(t), \hat{v}_c(t), \hat{x}_5(t), \hat{x}_6(t), \hat{x}_7(t)]$, input vector $\hat{u}(t) = [\hat{v}_g(t), \hat{v}_d(t), \hat{v}_{\text{ref}}(t), \hat{v}_{\text{off}}(t)]$ and output vector $\hat{y}(t) = \hat{v}_o(t)$, and is shown in (21), in the form $\left(\begin{smallmatrix} A & B \\ E & F \end{smallmatrix}\right)$.

All elements in the system model (21) shown at the bottom of this page, must be expressed as functions of definable system parameters and inputs only. Hence, the duty cycle D in (21) is expressed in terms of determinate elements by solving the quadratic equation (20), which is based on the equivalent steady-state model of the buck converter in Fig. 4. This modeling step serves to cater for system nonlinearities in the system model (21).

$$D^2 V_o \frac{R_{\text{in}}}{R} + D\left[-V_g - V_d + V_o\frac{(R_{\text{on}} - R_d)}{R}\right] + \left[V_d + V_o\frac{(R + R_d + R_l)}{R}\right] = 0 \tag{19}$$

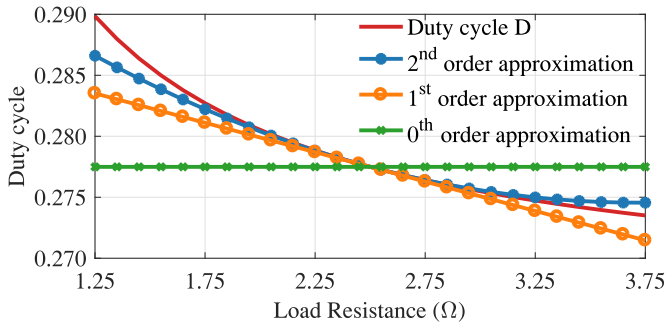

Fig. 5. Duty cycle D as a function of load R.

Further, all elements in the developed model must be in their rational forms in order to allow conversion of the system model to its corresponding LFT configuration. The duty cycle D in (14), which is obtained as a solution to (20), is irrational and is, therefore, approximated by a polynomial expansion. Fig. 5 shows the rational zeroth, first, and second-order Taylor series expansions of duty cycle D about the nominal operating point. Of note is that the nominal resistive load is 2.5 Ω as given in Table I, and the zeroth-order Taylor approximation of the duty cycle is 0.2768. Although the second-order Taylor series provides the best approximation, as can be seen in Fig. 5, the first-order approximation is used in this section, not to unnecessary increase the computational complexity.

It is to be added that all the elements of the developed model are rational, in symbolic form and expressed in terms of system parameters and system inputs only. The system model (21), as shown at the bottom of this page referred to as the linear equivalent model of the buck converter, is suited for μ analysis over a range of operating points and parameter variations [45], [46].

IV. System Model Refinement of the Experimental Prototype

The system model of the experimental buck converter shown in Fig. 3 has been built in Simulink environment. One of the initial objectives of the study was to obtain the refined system model of the experimental prototype to predict the behavior of

$$\left[\begin{array}{cccccccc|cccc}
\frac{-(R_{\text{cin}}+R_{\text{in}})}{L_{\text{in}}} & -\frac{1}{L_{\text{in}}} & \frac{DR_{\text{cin}}}{L_{\text{in}}} & 0 & p_1m_1 & p_1m_2 & p_1m_3 & \frac{1}{L_{\text{in}}} & 0 & p_1f_m & -p_1f_m \\
\frac{1}{C_{\text{in}}} & 0 & -\frac{D}{C_{\text{in}}} & 0 & p_2m_1 & p_2m_2 & p_2m_3 & 0 & 0 & p_2f_m & -p_2f_m \\
\frac{DR_{\text{cin}}}{L} & \frac{D}{L} & \frac{q}{L} & -\frac{R}{L(R+R_c)} & p_3m_1 & p_3m_2 & p_3m_3 & 0 & \frac{D-1}{L} & p_3f_m & -p_3f_m \\
0 & 0 & \frac{R}{C(R+R_c)} & -\frac{1}{C(R+R_c)} & 0 & 0 & 0 & 0 & 0 & 0 & 0 \\
0 & 0 & -\frac{R_cR}{R_c+R} & -\frac{R}{R_c+R} & -(w_{p2}+w_{p3}) & -w_{p2}w_{p3} & 0 & 0 & 0 & 1 & 0 \\
0 & 0 & 0 & 0 & 1 & 0 & 0 & 0 & 0 & 0 & 0 \\
0 & 0 & 0 & 0 & 0 & 1 & 0 & 0 & 0 & 0 & 0 \\
\hline
0 & 0 & \frac{R_cR}{R_c+R} & \frac{R}{R_c+R} & 0 & 0 & 0 & 0 & 0 & 0 & 0
\end{array}\right] \tag{20}$$

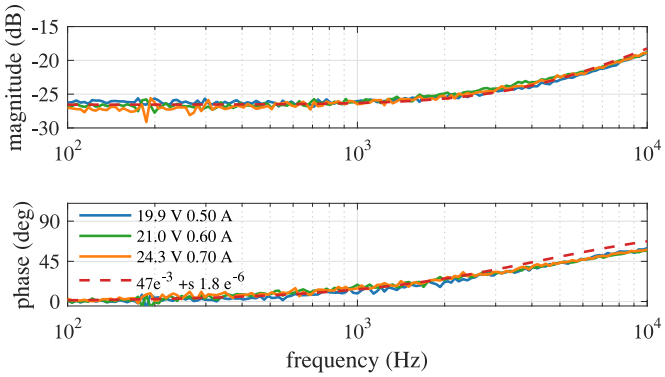

Fig. 6. Output impedance of power supply estimated through curve fitting of experimental measurements.

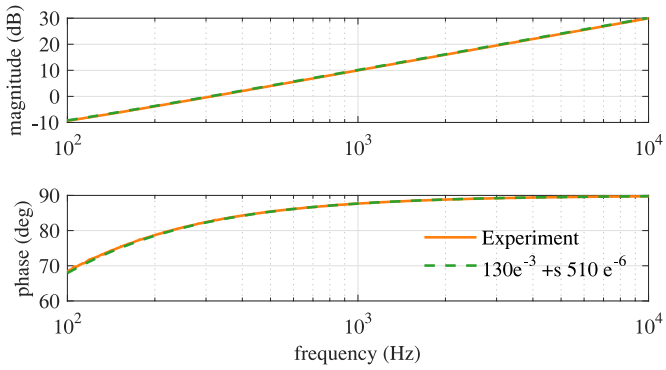

Fig. 7. Input filter inductance including measuring cable resistance estimated through curve fitting of experimental measurements.

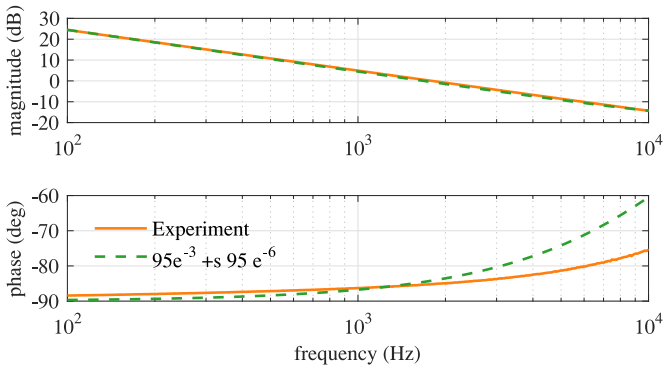

Fig. 8. Input filter capacitance estimated through curve fitting of experimental measurements.

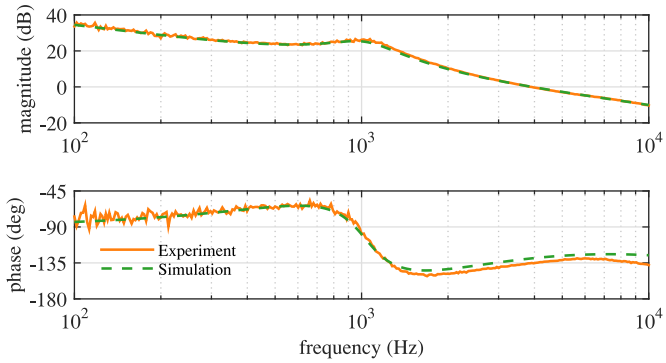

Fig. 9. Validation of simulation model loop gain against experimental measurements of loop gain.

the system such as borderline stability with fairly good accuracy. The procedure for refining the system model is done in three main stages, as described in this section.

A. Initial System Model

The first step consists in defining the initial average model of the buck converter under study based on available data and nameplate information, as defined under "the initial parameter values" in Table I. Many of these parameter values can be further refined to increase model fidelity.

B. Individual System Components Models

The second step of the process models individual system components through experimental measurements. It has been shown that nonidealities such as parasitic resistances in wiring and power supply, the equivalent series resistance (ESR) of the capacitors and inductors as well as, the voltage drop in the diode and the on-resistance of the switch transistor have significant impact on the accuracy of the model. The experimental measurements of a few system components are described below.

The output impedance of the power supply has been measured when connected to different loads and set to different voltages, as shown in Fig. 6. A network analyzer has been employed to obtain the dynamic measurements [50]. The best estimate of the experimental measurements of the power supply impedance, through curve fitting, is found to be $47e^{-3} + s1.8^{-6}$. From these measurements, the ESR and inductance of the power supply are estimated at $47\,\mathrm{m}\Omega$ and $1.8\,\mathrm{mH}$, respectively.

The input filter inductance and capacitance have been measured by means of an impedance analyzer. The measurements are depicted in Figs. 7 and 8, respectively. The filter inductance is estimated at 510 mH and after deducting the resistance of the cables used for the measurements of $70\,\mathrm{m}\Omega$, the ESR is estimated as $60\,\mathrm{m}\Omega$, as shown in Fig. 7. The input filter capacitance and ESR are estimated at $95\,\mu\mathrm{F}$ and $95\,\mathrm{m}\Omega$, respectively, as depicted in Fig 8. It is to be noted that although second-order polynomials provide better approximations, especially at high frequencies, the first-order approximation has been selected as it provides sufficient accuracy without unnecessarily complicating the model.

C. Refined System Model

The last step consists first of experimentally measuring the converter transfer functions, such as the loop gain T, the input impedance Z_i, and the output impedance Z_o, by means of a network analyzer [50]. The experimental measurements are then compared with the corresponding transfer functions obtained from the simulation model. The individual component model and the system model are refined and adjusted iteratively until a good match is obtained. Figs. 9 and 10 depict the loop gain and the input impedance of the converter obtained from both experiments and the updated simulation model. These

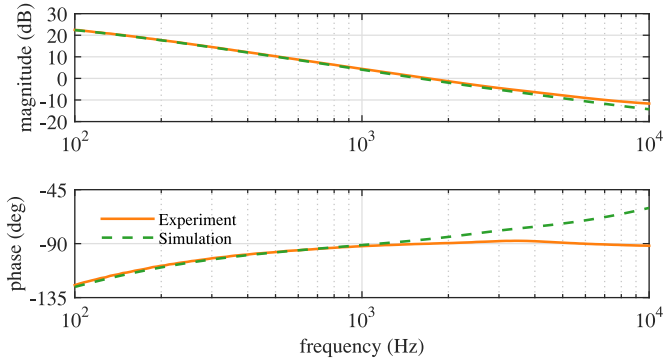

Fig. 10. Validation of simulation model input impedance against experimental measurements of input impedance.

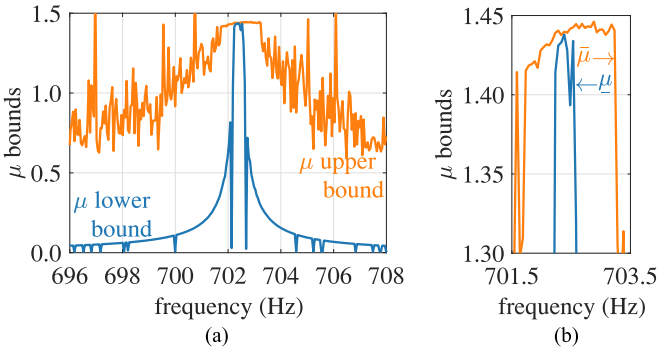

Fig. 11. Case 1.1—System with load uncertainty. (a) μ chart to predict critical R. (b) Zoomed area near the peak of the μ chart.

TABLE II
CASE 1.1—UNCERTAIN RESISTIVE LOAD

Parameter	Nominal value (R_o)	Range of variation (R_{var}) with respect to nominal value
R	2.5 Ω	± 50 %

TABLE III
CASE 1.1—SYSTEM WITH LOAD UNCERTAINTY, μ ANALYSIS RESULTS

Perturbation matrix	Robust stability margin ($1/\mu$)	μ	Critical load	
			R (Ω)	Power (W)
$\Delta(j \cdot 2\pi \cdot 702.4)$	0.696	1.44	1.63 Ω	16.0 W

measurements have been made without the input filter inductor and with a load of 1.6 Ω. The simulation model transfer functions match the experimentally observed behavior of the converter to good accuracy.

Through the process of model refinement, the "initial" values of the system components have been fine-tuned to their final values, as given by the "refined" values in Table I. The "refined" parameter values in Table I are used as nominal values for the equivalent system model (21) in μ analysis and to run simulations in Simulink for the case studies in Sections V–VII. The "initial" parameter values in Table I are used as nominal values for the case studies in Section VIII.

V. LOAD UNCERTAINTY

In this section, μ analysis is applied to determine the critical resistive load R that destabilizes the system as shown in Fig. 3. In this analysis, referred to as case study 1.1, the only uncertain parameter is load R that can vary around its nominal value by $\pm 50\%$ (i.e., $R_{\text{var}} = \pm 50\%$ as defined in (22)–(24) and Table II). The other system parameters are assumed to be constant with nominal values given as the "refined" values in Table I.

A. μ Analysis

Prior to μ analysis, the state-space model (21) is converted to its LFT form. In this paper, MATLAB Robust Stability Toolbox has been employed for performing both LFT and SSV analysis. Expressing (21) in the LFT form requires that all uncertain parameters be first converted to their LFT forms. In this case study, the uncertain element R has to be expressed as a function of its normalized form δ_R that lies between -1 and 1 as shown in (22). R_o and R_{var} can be derived from the minimum value ($R_{\min}$) and the maximum value ($R_{\max}$) of the resistive load as shown in (23) and (24) [48].

$$R = R_o + R_o R_{\text{var}} \delta_R \quad where \quad \delta_R \in [-1, 1] \tag{21}$$

$$R_o = (R_{\max} + R_{\min})/2 \tag{22}$$

$$R_{\text{var}} = (R_{\max} - R_{\min})/(R_{\max} + R_{\min}) \tag{23}$$

The normalized parameters δ_R are then extracted from the uncertain system model (21) and grouped in a diagonal matrix in a feedback form by applying the LFT technique. The resulting uncertainty matrix is shown in (25). δ_R appears 227 times in the Δ matrix, which corresponds to the number of times R appears in the system matrix.

$$\Delta(j \cdot 2\pi \cdot f) = \delta_R \; I_{227 \times 227} \tag{24}$$

μ analysis is then applied to the uncertain system model in LFT form by using MATLAB Robust Stability Toolbox. The results are shown in Fig. 11(a) and (b).

For this test, μ is equal to 1.44 as given by the peak value of the charts in Fig. 11(a) and (b). The smallest destabilizing matrix, of size 227×227 as given by (26), gives the robust stability margin ($1/\mu$) as 0.696 [49].

$$\Delta(j \cdot 2\pi \cdot 702.4) = -0.696 \; I_{227 \times 227} \tag{25}$$

By comparing (26) with (25), it can be noted that $\delta_R = -0.696$. The critical destabilizing load can be computed from $\delta_R = -0.696$ and (22) and is equal to 1.63 Ω or 16.0 W, as shown in (27) and Table III.

$$\begin{aligned} R &= R_o + R_o R_{\text{var}} \delta_R, \quad \text{where} \quad \delta_R \in [-1, 1] \\ &= 2.5 + 2.5 \times 50\% \times (-0.696) \\ &= 2.5 - 2.5 \times 35\% = 1.63 \end{aligned} \tag{26}$$

$\mu > 1$ indicates that the system is not robustly stable, i.e., the system does not remain stable over the whole uncertainty range

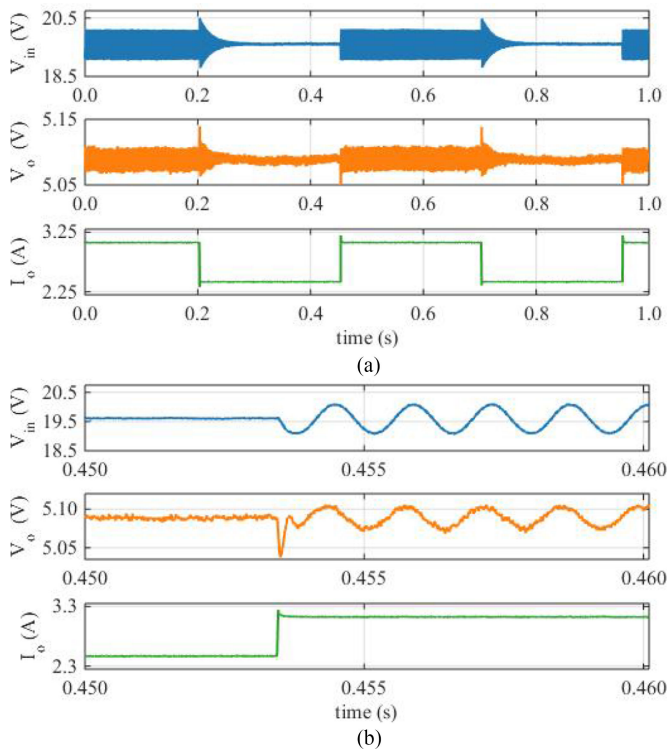

Fig. 12. Case 1.1—Experimental results for the system with load uncertainty. (a) System is at boundary of stability with $R = 1.63\ \Omega$ from $t = 0.453$ to 0.703 s. (b) Zoomed area near $t = 0.453$ s.

TABLE IV
CASE 1.1—SYSTEM WITH LOAD UNCERTAINTY, μ ANALYSIS, AND EXPERIMENTAL RESULTS

Uncertain load	Critical values		
	μ analysis	Simulation	Experiment
R (Ω)	1.63 Ω	1.61 Ω	1.62 Ω
Power (W)	16.0 W	16.1 W	16.1 W

between 1.25 and 3.75 Ω, as defined in Table II. In order to ensure that the system remains robustly stable, μ should be less than 1. This can be achieved by scaling the operating range of the system load by $1/\mu$, the robust stability margin. The robust uncertainty range of R is thus $2.5 \pm 2.5 \times 50\% \times 0.696$, i.e., $2.5\ \Omega \pm 35\%$.

B. Experimental Results

In this experiment, the electronic resistive load R was decreased in small steps from a peak value of 2 Ω until the system reached boundary stability. When R was decreased to 1.62 Ω at $t = 0.453$ s (i.e., I_o increased to 3.15 A), the system reached the boundary condition of stability, as shown by the sustained oscillations in V_{in} and V_o in Fig. 12(a) and (b). When R was increased back to 2 Ω at $t = 0.703$ s (i.e., I_o decreased to 2.55 A), the system stabilized again, as shown in Fig. 12(a). The critical load resistance of 1.62 Ω closely matches the value of 1.63 Ω predicted by μ analysis, as depicted in Table IV, with an error of 0.6%. It should be noted that, although the experimental results match closely the μ prediction, they are subject to measurement error.

TABLE V
CASES 1.1 AND 1.2—SYSTEM WITH LOAD UNCERTAINTY, EVALUATION OF POLYNOMIAL APPROXIMATIONS OF DUTY CYCLE D

Case study	D approximation	Robust stability margin ($1/\mu$)	Critical load	Size $\Delta(jw)$	Computation time
1.1	First order	0.696	1.63 Ω	227×227	34 min
1.2	Zeroth order	0.745	1.57 Ω	37×37	54 s

In addition, simulation was ran in the Simulink environment on the refined nonlinear model of the buck converter system under study. The simulation result of the critical load, as given in Table IV, fall within 1.2% of the μ prediction, and the discrepancy may be accounted for by uncertainties in the model such as the approximation error of duty cycle D. Model uncertainties can be considered in the robust stability analysis, as is demonstrated later in Section VIII.

C. Computation Time

In order to assess the effect of the duty cycle approximation on robust stability margin and computation time, μ analysis has also been performed by using the zeroth-order approximation of the duty cycle D, referred to as case study 1.2 in Table V. The analyzes, with zeroth- and first-order approximation of the duty cycle D, have been performed using a frequency grid of 250 points between 650 and 750 Hz on an Intel Core i7-3820 3.6 GHz processor with 32GB RAM. The μ results and the computation times are given in Table V. The zeroth-order approximation introduces an error of 7% in the robust stability margin and an error of 4% in the critical load R, with respect to the first-order approximation. In spite of the loss in accuracy, the computation time is seen to reduce considerably, as noted in Table V. This is due to the fact that D appears 189 times in the system model. By setting D as a constant, the size of the uncertainty matrix reduces from 227×227 to 37×37. It can be inferred that the size of the uncertainty matrix has a key influence on computational cost. Of note is that nonlinear terms can be treated as uncertain elements of the system, as will be examined in section VIII.

VI. LOAD AND LINE RESISTANCE UNCERTAINTIES

In practice, the actual parameter values of system components may differ at the assembly stage when compared to initial design values. These parametric uncertainties may lead to system instability. This section considers the case when the load and the line resistance of the analyzed system are not known accurately, but are known to lie within certain ranges, as defined in Table VI. The μ tool can be used to determine the bounds within which these uncertain parameters must lie in order to guarantee stability of the system under study. The other system parameters are fixed and given by the "refined" values in Table I.

TABLE VI
CASE 2.1—UNCERTAIN LOAD AND LINE RESISTANCE

Uncertain parameters	Nominal value	Range of variation with respect to nominal value
R	$R_o = 2.5\ \Omega$	$R_{\text{var}} = \pm 50\%$
R_{in}	$R_{\text{ino}} = 0.3\ \Omega$	$R_{\text{invar}} = \pm 50\%$

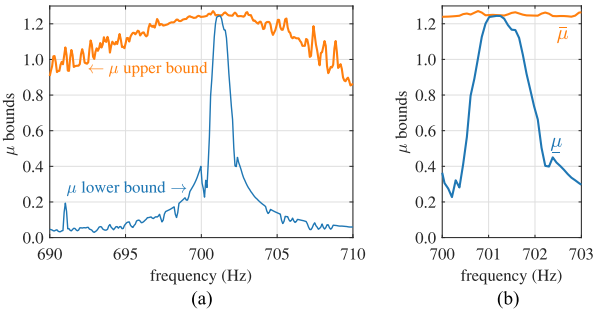

Fig. 13. Case 2.1—System with load and line resistance uncertainties. (a) μ chart to predict critical load R. (b) Zoomed area near the peak of the μ chart.

A. μ Analysis

μ analysis is performed on the system model (21), by using the first-order Taylor series approximation of the duty cycle D with respect to both R and R_{in}. The peak value of μ is equal to 1.24, and occurs at a frequency of 701.3 Hz, as can be seen in Fig. 13(a) and (b). The robust stability margin $(1/\mu)$ is 0.803. The general uncertainty matrix is given by (28) and the critical uncertainty matrix obtained from μ analysis is shown in (29). By comparing (28) and (29), δ_R and δ_{Rin} are found to be equal to -0.803. The critical values of R and R_{in} can be computed as 1.50 and 1.18 Ω, respectively, from the aforementioned δ_R and δ_{Rin} values and the general equation (1). This case study shows that if the values of R and R_{in} are kept within 80.3% of their respective nominal values, the system is ensured to be robustly stable. It can be noted that the robust stability margin in case 2.1 is increased with respect to case 1.1, as the line resistance R_{in} is set in the range [150 mΩ, 450 mΩ], and in that can provide more damping to the input LC filter.

$$\Delta(j \cdot 2\pi \cdot f) = \text{diag}(\delta_R I_{227},\ \delta_{\text{Rin}} I_{217}) \tag{27}$$

$$\Delta(j \cdot 2\pi \cdot 701.3) = \text{diag}(-0.803 I_{227},\ -0.803 I_{217}) \tag{28}$$

B. Experimental Results

In order to validate the μ predictions of the case study 2.1, a set of experiments were performed on the buck converter system. By keeping R_{in} around 0.18 Ω, the load was slowly decreased until the system became unstable. The experimental results are shown in Fig. 14. When R is set at 1.89 Ω, the system stabilizes, as shown in the top chart in Fig. 14. When R is decreased to 1.54 Ω, the system reaches boundary stability, as shown by the sustained oscillations in the input voltage V_{in} in the middle chart in Fig. 14. Decreasing R to 1.50 Ω causes the system to become unstable, as shown in the bottom chart in Fig. 14. The line resistance R_{in}, used in the experiment, has been accurately measured

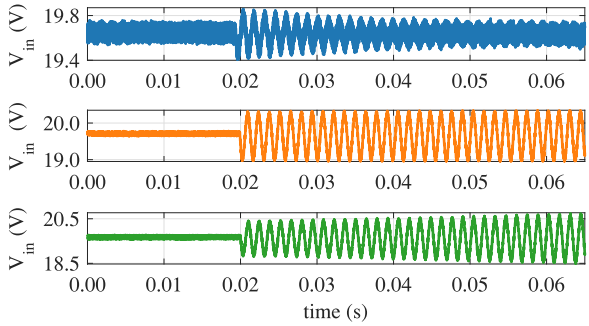

Fig. 14. Case 2.1—Experimental results for system with uncertain R with $R_{\text{in}} = 185\,\text{m}\Omega$. (a) Top chart: System is stable with $R = 1.89\ \Omega$. (b) Middle chart: System is at boundary of stability with $R = 1.54\ \Omega$. (c) Bottom chart: System is unstable with $R = 1.50\ \Omega$.

TABLE VII
CASE 2.1—SYSTEM WITH LOAD AND LINE RESISTANCE UNCERTAINTIES, μ ANALYSIS, SIMULATION, AND EXPERIMENTAL RESULTS

Uncertain parameters	Critical values		
	μ analysis	Simulation	Experiment
R (Ω)	1.50	1.49	1.54
R_{in} (Ω)	0.180	0.179	0.185

and found to be 1.85 Ω. The experimental results, summarized in Table VII, are in close agreement with the μ predictions, with an error falling within 3%, and the discrepancy may be accounted for by measurement error and some uncertainties in the system model.

It is to be added that the Simulink model of the system, which is based on the state-space model used in μ analysis, has also been used to verify the μ analysis results. The simulation results from the Simulink model closely match the μ predictions as shown in Table VII, and the discrepancy may be accounted for by some uncertainties in the model such as the approximation error of duty cycle D. The effect of model uncertainties on the system stability margins is analyzed in Section VIII.

VII. TEMPERATURE UNCERTAINTY

Although a power system can be modeled to good accuracy, however, in practice, the values of its system components are bound to vary during operation. Temperature is one of the main factors that can introduce uncertainties in multiple system parameters. In this section, the μ approach is applied to the buck converter, as shown in Fig. 3, when it is exposed to large temperature variation, based on the methodology used in Section V. The duty cycle D is estimated by its zeroth-order approximation. The μ predictions are thereafter evaluated against the μ results from case study 1.2 in Section V in order to investigate the effect of extreme temperature variation on the robust stability margin.

A. Uncertain Parameters

In this analysis, referred to as case study 3.1, the buck converter is considered to be working in an environment where the

TABLE VIII
CASE 3.1—UNCERTAINTIES IN LOAD AND TEMPERATURE

Uncertain parameters	Nominal value	Range of variation with respect to nominal value
T	$T_o = 20\,^{\circ}\text{C}$	$\Delta T = \pm 60\,^{\circ}\text{C}$
R_{es}	R_{eso}	$R_{\text{esvar}} = \alpha\,\Delta\text{T} = \pm 24\%$
R	R_o =2.5 Ω	$R_{\text{var}} = \pm 50\%$

TABLE IX
SYSTEM WITH LOAD AND TEMPERATURE UNCERTAINTY—μ ANALYSIS RESULTS FOR LOAD

Uncertain parameter	Robust stability margin	μ	Critical load	
			R (Ω)	Power (W)
Load	0.505	1.98	1.87 Ω	13.9 W

temperature may vary between -40 and 80 °C with a reference value of 20 °C, as shown in Table VIII.

The variations in temperature may influence the characteristics of the resistive components of the buck converter, which include but are not limited to the system parasitics and cable resistances. These components, which are denoted as R_{es} further in the text and comprising R_{in}, R_{cin}, R_l, R_{on}, R_c, may have different temperature coefficients depending on their constituent materials. However, for the sake of simplicity, a temperature coefficient of resistance (α) of 0.004/°C as for a copper wire is assumed for the aforementioned components in this paper. From (30) and Table VIII, it can be seen that the variations in temperature (T) of ±60 °C cause variations in the resistive components of ±24% around their nominal values denoted as R_{eso}.

$$R_{\text{esvar}} = (R_{\text{es}} - R_{\text{eso}})/R_{\text{eso}} = \alpha\Delta T \tag{29}$$

The nominal values of the system components, including R_{es}, are given as the "refined" values in Table I. It is assumed that the resistive load varies within ±50% of its nominal value, as in case 1.1 in Section V, and as depicted in Table VIII. The μ approach is applied to study the effect of the defined temperature variation on stability robustness of the analyzed system.

B. μ Analysis

By employing LFT technique, the system model (21) is first expressed in the LFT form. The structure of the resulting uncertainty matrix is shown in

$$\Delta(j\cdot 2\pi\cdot f) = \text{diag}(\delta_R I_{41},\ \delta_{\text{Rc}} I_{13},\ \delta_{\text{Rcin}} I_{38},\ \delta_{\text{Rin}} I_{25},\ \delta_{\text{Rl}} I_{23},\ \delta_{\text{Ron}} I_{27}). \tag{30}$$

The μ approach is then applied to the uncertain system model in its LFT form. The μ chart is depicted in Fig. 15, where the peak of the μ lower bound is seen to be equal to 1.98 at the critical frequency of 704 Hz.

The corresponding critical values of the resistive load and resistive components, calculated from the μ bounds, are given in Table X. The critical destabilizing load is now 1.87 Ω (13.9 W),

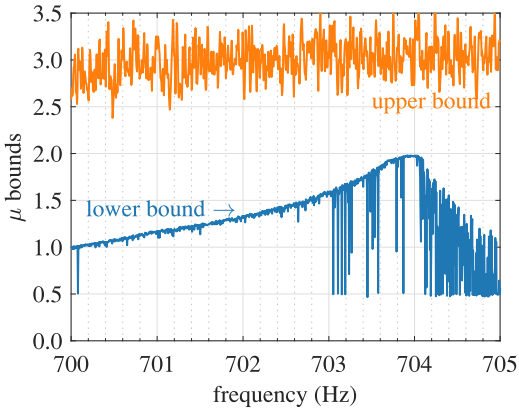

Fig. 15. Case 3.1—System with load and temperature uncertainties, μ chart to predict load R and critical resistive components R_{es}.

TABLE X
CASE 3.1—SYSTEM WITH LOAD AND TEMPERATURE UNCERTAINTIES, μ ANALYSIS, AND TIME-DOMAIN SIMULATION RESULTS

Uncertain parameters	Nominal value	Critical values	
		μ analysis	Simulation
R (Ω)	2.50	1.87	1.87
R_c (mΩ)	17	14.9	14.9
R_{cin} (mΩ)	95	83.5	83.5
R_{in} (mΩ)	160	140.6	140.6
R_l (mΩ)	50	43.9	43.9
R_{on} (mΩ)	160	154.7	154.7

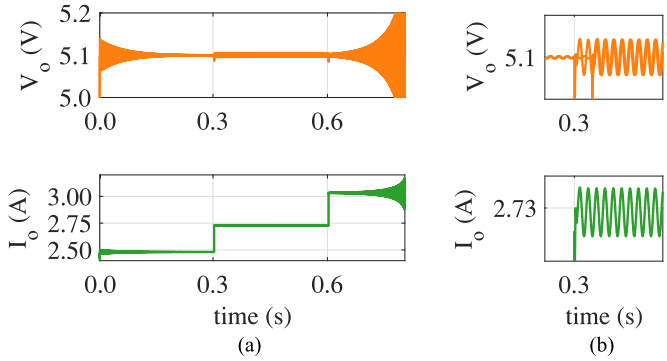

Fig. 16. Case 3.1—System with load and temperature uncertainties. (a) Top figure—voltage v_o, bottom figure—current i_o. (a) At $t = 0$ s, $R = 1.1 \times 1.87$ Ω. (b) At $t = 0.3$ s, $R = 1.87$ Ω. (c) At $t = 0.6$ s, $R = 0.9 \times 1.87$ Ω, where $R = 1.87$ Ω is the critical load predicted by μ analysis. (b) Zoomed area near $t = 0.3$ s.

based on the μ lower bound. This represents a robust stability margin of 0.505, as shown in Table IX.

C. Simulation Verification

The refined Simulink model of the buck converter is used to verify the μ analysis results obtained in the earlier section. When the critical values predicted by μ analysis, as given in Table X, are input in the Simulink model of the buck converter, the system reaches boundary stability. Fig. 16(a) and (b) shows

TABLE XI
CASES 3.1 AND 1.2—EFFECT OF TEMPERATURE ON ROBUST STABILITY MARGIN WITH D CONSTANT

Case study	Temperature considered	Critical load		Robust stability margin
		R (Ω)	power (W)	
3.1	Yes	1.87 Ω	13.9 W	0.505
1.2	No	1.57 Ω	16.6 W	0.745

the results for the case where the load R is varied with the other R_{es} components fixed at their critical values given in Table X.

When R is set to be 10% higher than its critical value of 1.87 Ω at $t = 0$ s (i.e., I_o is 2.48 A), the system stabilizes as shown in Fig. 16(a). When R is decreased to the critical value of 1.87 Ω at $t = 0.3$ s (i.e., I_o is 2.73 A), the system reaches boundary stability condition, as can be seen from the sustained oscillations in V_o in Fig. 16(a) and (b). When R is decreased by a further 10% below 1.87 Ω at $t = 0.6$ s (I_o is 3.03 A), the system becomes unstable. The simulation results closely match the results predicted by μ analysis as shown in Table X.

D. Results Analysis

From robust stability analysis, $\mu > 1$ indicates that the system under investigation, with 50% load uncertainty, is not guaranteed to remain stable over the whole range of variation of temperature (i.e., -40 to 80 °C). Based on the examination of the hypercube concept presented in Section II, the buck converter system under study remains robustly stable within a hypercube of the sixth-order dimension, of coordinate size $\mu = 0.505$, and centered about the nominal point. Any combination of parameter values chosen within the aforementioned hypercube will ensure the robust stability of the buck converter under study, within the range of temperature variation defined in Table VIII. As depicted in Table XI, when the uncertainty in temperature is considered, the robust stability margin is 0.505. When temperature variation is neglected, the robust stability margin is 0.745, as shown in case study 1.2 and Table V. This represents 32% decrease in the robust stability margin, as shown in Table XI. The duty cycle D is constant in both cases 3.1 and 2.1. This study confirms that the variation in temperature can have a significant influence on robust stability margin and must, therefore, be incorporated in the stability assessment.

VIII. MODEL UNCERTAINTIES

In practice, it is neither viable nor time-efficient to create highly refined system models to represent actual systems. Hence, approximate system models, with a good tradeoff between accuracy and simplicity, are often used for design. The nominal values of their system components are generally based on known data such as nameplate information. This section aims to demonstrate how model uncertainties, which may be known to different level of accuracy, can be incorporated in robust stability analysis without compromising the reliability of the results. In addition, it examines the effect of model uncertainties on robust stability margin.

TABLE XII
CASES 4.1, 4.2, 4.3—UNCERTAINTIES IN LOAD AND SYSTEM MODEL

Uncertain parameters	Nominal value	Range of variation		
		Case 4.1	Case 4.2	Case 4.3
R	2.50 Ω	$\pm$ 50%	$\pm 50\%$	$\pm 50\%$
R_{in}	135 mΩ	–	$\pm 50\%$	$\pm 30\%$
L_{in}	480 μH	–	$\pm 50\%$	$\pm 30\%$
C_{in}	100 μF	–	$\pm 10\%$	$\pm 6\%$
R_{cin}	80 mΩ	–	$\pm 10\%$	$\pm 6\%$
L	42 μ H	–	$\pm 50\%$	$\pm 30\%$
R_l	45 mΩ	–	$\pm 10\%$	$\pm 6\%$
C	590 μ F	–	± 50 %	$\pm 30\%$
R_c	10 mΩ	–	$\pm 10\%$	$\pm 6\%$
D	0.2768	–	$\pm 4.5\%$	$\pm 4.5\%$

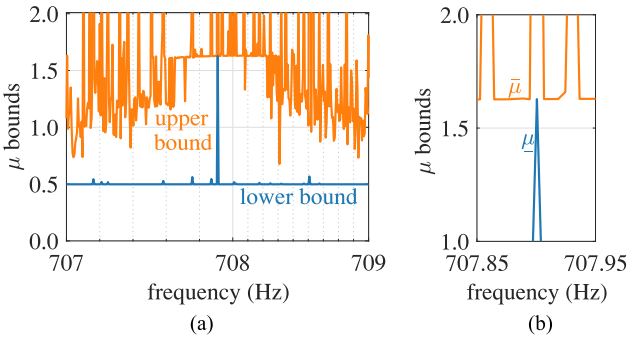

Fig. 17. Case 4.1: System with load uncertainty and no model uncertainty. (a) μ chart to predict critical load R. (b) Zoomed area near the peak of the μ chart.

The approach is illustrated by applying it to the buck converter example power system in Fig 3. The "initial" values of the system components, as given in Table I, are used as the nominal values for μ analysis. Three cases are investigated, as defined in Table XII. In case 4.1, robust stability margin is evaluated without taking into account any uncertainties in the model. Only uncertainty in the load is considered. In cases 4.2 and 4.3, uncertainties in the model are included in the analyses. However, the approximation errors in the model in case 4.2 are larger as compared with those in case 4.3. The other system parameters are considered to be fixed as defined by the "initial" parameter values in Table I.

A. System With No Model Uncertainty

This section evaluates the robust stability margin for case 4.1. μ analysis is applied to the system model (21) with the uncertain parameters as defined in Table XII. The μ chart, as depicted in Fig. 17(a) and (b), shows that the μ lower bound is 1.63. This corresponds to a robust stability margin of 0.614 and a critical load of 1.73 Ω or 15 W, as shown in Table XIII. The buck converter is predicted to remain stable for an output power of up to 15 W.

B. System With Model Uncertainties

The stability robustness for cases 4.2 and 4.3 are evaluated in this section. The maximum possible errors that may be ex-

TABLE XIII
CASE 4.1—SYSTEM WITH LOAD UNCERTAINTY AND NO MODEL UNCERTAINTY, μ ANALYSIS RESULTS FOR LOAD

Uncertain parameter	Robust stability margin	$\underline{\mu}$	Critical load	
			R (Ω)	power (W)
Load	0.614	1.63	1.73 Ω	15.0 W

TABLE XIV
CASES 4.1, 4.2, 4.3—SYSTEM WITH LOAD AND MODEL UNCERTAINTIES—μ ANALYSIS RESULTS FOR LOAD

Case study	Model uncertainties	Robust stability margin	$\underline{\mu}$	Critical load	
				R (Ω)	power (W)
4.1	No	0.614	1.63	1.73 Ω	15.0 W
4.2	Yes	0.210	4.76	2.24 Ω	11.6 W
4.3	Yes	0.288	3.47	2.14 Ω	12.2 W

pected in the nominal values, as given in Table XII, are taken into account in the analyses. This is based on the knowledge of the system. For instance, for case 4.2, the tolerances of the capacitors and inductors are known to be well within 10% of their nominal values. Parasitic elements, which may be nonlinear in nature, are generally hard to quantify. Hence, the system parasitics such as the ESR of the inductors and capacitors, have been considered to vary within a maximum range of $\pm 50\%$ within their estimated nominal values. Further, nonlinear terms in the system model may be treated as uncertain elements. Hence in this case, the duty cycle D is set as an uncertain parameter with 4.5% uncertainty, based on its maximum variation range as depicted in Fig. 5. This eliminates the need for high-order approximations, which has the added advantage of reducing the size of the uncertainty matrix. As in previous case studies, the load R is considered to vary within 50% of its nominal value. In case 4.3, it is considered that the values of the uncertain parameters are known with better accuracy, with variation ranges of the system inductances, capacitors and ESRs being tighter, as depicted in Table XII.

μ analysis is applied to the system model (21) based on the uncertain parameters defined in Table XII, for cases 4.2 and 4.3. Following the LFT operation, the structure of the uncertainty matrix, of size 351×351, is obtained as

$$\Delta(j \cdot 2\pi \cdot f) = \text{diag}(\delta_C I_2,\ \delta_{\text{Cin}} I_6,\ \delta_D I_{189},\ \delta_L I_4,\ \delta_{\text{Lin}} I_8,\ \delta_R I_{41}, \delta_{\text{Rc}} I_{13},\ \delta_{\text{Rcin}} I_{39},\ \delta_{\text{Rin}} I_{25},\ \delta_{\text{Rl}} I_{24}). \tag{31}$$

The μ charts for cases 4.2 and 4.3 are shown in Fig. 18(a) and (b), respectively. The μ lower bound is 4.76 for case 4.2. This corresponds to a robust stability margin of 0.21 and a critical load of 2.24 Ω or 11.6 W, as depicted in Table XIV. For case 4.3, the μ lower bound is 3.47. The associated robust stability margin is 0.288, and the critical load is 2.14 Ω or 12.2 W. The results are shown in Table XIV. Thus, after taking into account the aforementioned uncertainties in the model, the buck converter is predicted to remain stable for an output power of up to 11.6 W for case 4.2, and up to 12.2 W for case 4.3, as shown in

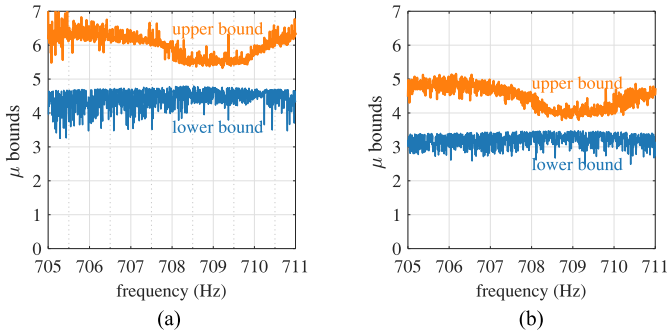

Fig. 18. Cases 4.2 and 4.3—System with load and model uncertainties, μ charts to predict critical load R for (a) case 4.2 and (b) case 4.3.

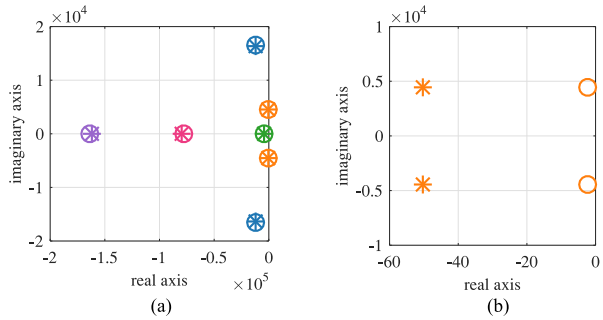

Fig. 19. Case 4.2: System with load and model uncertainties. (a) Plot of eigenvalues based on μ lower bound predictions, (*) eigenvalues with nominal parameters, (o) eigenvalues with critical parameters. (b) Zoomed view near the imaginary axis.

TABLE XV
CASES 4.1, 4.2, 4.3—SYSTEM WITH LOAD AND MODEL UNCERTAINTIES, μ ANALYSIS RESULTS, AND COMPUTATION TIME

Case study	Model uncertainties	Robust stability margin ($1/\mu$)	Critical load	Size $\Delta(jw)$	Computation time
4.1	No	0.614	1.73 Ω	37×37	9 s
4.2	Yes	0.210	2.24 Ω	351×351	3.4 h
4.3	Yes	0.288	2.14 Ω	351×351	3.6 h

Table XIV. The results for case 4.1 are included in Table XIV for completion.

With the aim of verifying the μ results, the eigenvalues of the nominal model of the linear equivalent model (21) are evaluated against the eigenvalues of the critical linear equivalent model for case 4.2, obtained from the critical parameter values predicted by μ analysis. The corresponding plots of the eigenvalues are depicted in Fig. 19(a) and (b). It can be noted that applying the critical values, predicted by μ analysis, brings the eigenvalues near to the imaginary axis. This confirms that μ analysis has identified the critical values at the boundary of stability.

C. Results Analysis

The robust stability margins ($1/\mu$) for cases 4.1, 4.2, and 4.3 are depicted in Table XIV. It is interesting to note that the stability robustness for cases 4.1, 4.2, and 4.3 is represented by hypercubes, of the tenth-order dimension, centered about the nominal point, but of sizes 0.614, 0.210, and 0.288, respectively.

TABLE XVI
SUMMARY OF RESULTS

Case study	Uncertain parameters	Duty cycle D	Nominal values	Robust stability margin	μ	Critical load	
						R (Ω)	power (W)
1.1	Load R	First-order approximation	Refined	0.696	1.44	1.63 Ω	16.0 W
1.2	Load R	Zeroth-order approximation	Refined	0.745	1.34	1.57 Ω	16.6 W
2.1	Load R and line resistance R_{in}	First-order approximation	Refined	0.803	1.24	1.50 Ω	17.3 W
3.1	Load R and temperature T	Zeroth-order approximation	Refined	0.505	1.98	1.87 Ω	13.9 W
4.1	Load R and no model uncertainty	Zeroth-order approximation	Initial	0.614	1.63	1.73 Ω	15.0 W
4.2	Load R and model uncertainties (wide range)	D uncertain parameter	Initial	0.210	4.76	2.24 Ω	11.6 W
4.3	Load R and model uncertainties (narrow range)	D uncertain parameter	Initial	0.288	3.47	2.14 Ω	12.2 W

When uncertainties are not included in the model, the analyzed system has the largest hypercube with a robust stability margin of 0.614, as depicted in Table XIV. Although, the results may seem to be less conservative, they cannot be guaranteed to be reliable, as the nominal parameters are rough estimates. With model uncertainties incorporated in the analysis, the robust stability margin is 0.210 and 0.288 for cases 4.2 and 4.3, respectively, representing smaller hypercubes with respect to case 4.1. Although the results for cases 4.2 and 4.3 seem to be conservative in comparison to case 4.1, they are more reliable. This is because the analyses take into account uncertainties of the system model, and therefore, include worst case scenarios.

Further, in case 4.2, the parametric space within which the system under study is robustly stable is smaller than in case 4.3, as given by the aforementioned hypercubes. These findings indicate that the larger the uncertainty range, the tighter is the resulting robust stability margin, and the smaller the hypercube. While the size of their hypercubes, which represent the parametric space within which the systems are robustly stable, may differ, the results are reliable in both the cases since they include model uncertainties. It is to be pointed out that the reliability of the results is still dependent on the validity of the defined bounds of the uncertain system parameters.

Of note is that incorporating model uncertainties is computationally more expensive. This is evident since the size of the uncertainty matrix increases with the number of uncertain parameters. However, it is to be noted that the computation time is also dependent on the defined frequency grid. For very large uncertainty matrices, the computation time can be kept reasonably low by initially using a frequency grid of low density over a wide range of frequencies so as to obtain an estimated critical frequency value. μ analysis is then performed by narrowing the frequency range around the estimated critical frequency but keeping the initial number of frequency points. The analysis is eventually performed around the peak of the μ chart; this process may be repeated with higher number of frequency points over the very narrow frequency range until the μ values returned by the analyses remain consistent. For the case studies in this section, the μ results and computation times are given in Table XV, based on a frequency grid of 25 points between 707 and 708 Hz for case 4.1; 708 and 709 Hz for case 4.2; and 709 and 710 Hz for case 4.3. The analyses were performed on a Intel Core i7-3820 3.6 GHz processor with 32GB RAM.

The section of this paper has important implications. Often times, the design engineer does not have sufficient information as to the exact values of the system components. Yet, the parameters may be estimated within some reasonable bounds. With the μ approach, the designer is offered the flexibility of determining the best tradeoff between accuracy and practicality, by choosing the levels of details that are incorporated into modeling, depending on available information. The same system model is employed. Only the considered uncertain elements are defined differently.

IX. SUMMARY OF RESULTS

In practice, PE systems are subject to variations in load, line resistance, and operating temperature while their nominal system model is generally bound to contain parametric model uncertainties. This paper has applied the μ tool to gauge the impact of the aforementioned uncertainties on the robust stability margin of the dc/dc buck converter system. The results are depicted in Table XVI. In the case study 1.1, μ analysis has determined that the example system becomes unstable when the output power is increased to 16 W. It has been found in case study 2.1 that if the uncertain parameters R and R_{in} are kept within 80.3% of their respective nominal values, the system under study can be ensured to be stable for an output power of up to 17.3 W. For the case 2.1, the robust stability margin increases as the source resistance R_{in}, set in the range of [150 mΩ, 450 mΩ], provides more damping to the resonant LC input filter with respect to case 1.1, when R_{in} is set at a constant value of 160 mΩ. The μ predictions for case studies 1.1 and 2.1 are supported by experimental results. Further, the robust stability margin of the buck converter has been found to be 74.5% when uncertainties in temperature are not included in case study 1.2, as compared to 50.5% when uncertainties in temperature are included as shown in case study 3.1. The findings emphasize the necessity of incorporating operating conditions uncertainties for more reliable stability analysis of a system. The study has also demonstrated how the μ tool can be employed to account for model uncertainties, including certain classes of nonlinearities in the system model, such as in duty cycle D in this paper. μ analysis has predicted the critical output power of the considered buck converter to be 15.0 W, when model uncertainties are neglected in case study 4.1. On the other hand, the critical output power has been determined as 11.6 W in case study 4.2, when uncertainties are included, while

its value increased to 12.2 W, when the given uncertainties are defined within a relatively narrower range in case study 4.3. As discussed in Section II, although $\underline{\mu}$ is not guaranteed to be equal to μ, it is generally close to μ. For the cases investigated in this paper, as the $\underline{\mu}$-based predictions match closely the results from experiment, time-domain simulations and eigenplots, it can be inferred that the lower bound $\underline{\mu}$ is a good estimate of μ.

X. Conclusion

This paper has demonstrated practical approaches to applying the μ method in the assessment of robust stability of PE systems with single and multiple uncertainties, based on the widely employed dc/dc buck converter system. Further, it has shown the necessity of incorporating uncertainties in stability analysis. The μ tool has been used to determine the bounds within which the uncertain load must lie in order to guarantee the stability of the system under study. The analysis has been extended to include line resistance uncertainty. The μ predictions of the critical destabilizing resistive load of the system under study, with and without line resistance uncertainty, have been validated in the experiment. It has been shown how accounting for variation in operating temperature, which has an effect on multiple resistive system components, can increase the reliability of stability assessment. Further, the practical approach of including uncertainties, such as in parasitics and nonlinearity in duty cycle, in the nominal system model has been demonstrated. Although the robust stability margin has been found to be tighter when uncertainties are defined within wider ranges or with less accuracy, the work has shown that the results can be employed reliably as worse case scenarios are accounted for, which is particularly important for safety critical applications. In addition, the methodology for applying the μ tool as well as the interpretation of the μ results have been presented in a generalized and clear manner, which allows it to be extended to wider applications, and to include yet further sources of uncertainties.

Acknowledgement

This project has been conducted in the frame of the Clean Sky 2 Joint Undertaking under the European Union's Horizon 2020 research and innovation programme under grant agreement N° CS2-SYS-GAM-2014-2015-01.

References

[1] I. E. Agency, "Transport energy and CO_2: Moving towards sustainability," 2009. [Online]. Available: https://www.iea.org/publications/freepublications/publication/transport2009.pdf

[2] H. Zhang, C. Saudemont, B. Robyns, and M. Petit, "Comparison of technical features between a more electric aircraft and a hybrid electric vehicle," in *Proc. 2008 IEEE Veh. Power Propulsion Conf.*, Sep. 2008, pp. 1–6.

[3] R. D. Middlebrook, "Input filter considerations in design and application of switching regulators," in *Proc. IEEE Ind. Appl. Soc. Ann. Meeting*, 1976, pp. 366–382.

[4] A. B. Jusoh, "The instability effect of constant power loads," in *Proc. Nat. Power Energy Conf.*, 2004, pp. 175–179.

[5] A. Emadi, A. Khaligh, C. H. Rivetta, and G. A. Williamson, "Constant power loads and negative impedance instability in automotive systems: Definition, modeling, stability, and control of power electronic converters and motor drives," *IEEE Trans. Veh. Technol.*, vol. 55, no. 4, pp. 1112–1125, Jul. 2006.

[6] A. M. Rahimi and A. Emadi, "An analytical investigation of dc/dc power electronic converters with constant power loads in vehicular power systems," *IEEE Trans. Veh. Technol.*, vol. 58, no. 6, pp. 2689–2702, Jul. 2009.

[7] S. Rosado, R. Burgos, F. Wang, and D. Boroyevich, "Large-signal stability analysis in power systems with a synchronous generator connected to a large motor drive," in *Proc. 2007 IEEE Elect. Ship Technol. Symp.*, May 2007, pp. 42–47.

[8] A. Riccobono and E. Santi, "Comprehensive review of stability criteria for DC power distribution systems," *IEEE Trans. Ind. Appl.*, vol. 50, no. 5, pp. 3525–3535, Sep./Oct. 2014.

[9] G. F. Franklin, J. D. Powell, A. Emami-Naeini, and J. D. Powell, *Feedback Control of Dynamic Systems*, vol. 2. Reading, MA, USA: Addison-Wesley, 1994.

[10] R. C. Dorf and R. H. Bishop, *Modern Control Systems*. Reading, MA, USA: Addison-Wesley, 1998.

[11] K. Areerak, "Modelling and stability analysis of aircraft power systems," Ph.D. dissertation, The Dept. Elect. Electron. Eng., Univ. Nottingham, Nottingham, U.K., 2009.

[12] W. E. Sollecito and D. A. Swann, "Computer evaluation of high-temperature aircraft a-c electrical system designs," *Trans. Amer. Inst. Elect. Eng. Part II: Appl. Ind.*, vol. 78, no. 6, pp. 434–444, Jan. 1960.

[13] J. Doyle, "Analysis of feedback systems with structured uncertainties," *Proc. Inst. Elect. Eng. D—Control Theory Appl.*, vol. 129, no. 6, pp. 242–250, 1982.

[14] K. Zhou, J. Doyle, and K. Glover, *Robust and Optimal Control*. Englewood Cliffs, NJ, USA: Prentice-Hall, 1996.

[15] M. Davari and Y. A. R. I. Mohamed, "Robust multi-objective control of VSC-based dc-voltage power port in hybrid ac/dc multi-terminal microgrids," *IEEE Trans. Smart Grid*, vol. 4, no. 3, pp. 1597–1612, Sep. 2013.

[16] M. Davari and Y. A. R. I. Mohamed, "Dynamics and robust control of a grid-connected VSC in multiterminal dc grids considering the instantaneous power of dc- and ac-side filters and dc grid uncertainty," *IEEE Trans. Power Electron.*, vol. 31, no. 3, pp. 1942–1958, Mar. 2016.

[17] S. Sudhoff and O. Wasynczuk, "Analysis and average-value modeling of line-commutated converter-synchronous machine systems," *IEEE Trans. Energy Convers.*, vol. 8, no. 1, pp. 92–99, Mar. 1993.

[18] M. Kuhn, Y. Ji, and D. Schrder, "Stability studies of critical DC power system component for more electric aircraft using mu sensitivity," in *Proc. IEEE Mediterranean Conf. Control Autom.*, 2007, pp. 1–6.

[19] J. Elizondo, R. Y. Zhang, J. K. White, and J. L. Kirtley, "Robust small signal stability for microgrids under uncertainty," in *Proc. 2015 IEEE 6th Int. Symp. Power Electron. Distrib. Gener. Syst.*, 2015, pp. 1–8.

[20] P. M. Young, M. P. Newlin, and J. C. Doyle, "μ analysis with real parametric uncertainty," in *Proc. 30th IEEE Conf. Decis. Control*, 1991, pp. 1251–1256.

[21] R. Tymerski, "Worst case stability analysis of switching regulators using the structured singular value," in *Proc. 25th Annu. IEEE Power Electron. Spec. Conf.* vol. 1, Jun. 1994, pp. 281–288.

[22] M. Green and D. J. Limebeer, *Linear Robust Control*. North Chelmsford, MA, USA: Courier Corporation, 2012.

[23] S. Skogestad and I. Postlethwaite, *Multivariable Feedback Control: Analysis and Design*. Hoboken, NJ, USA: Wiley, 2005.

[24] A. Packard and J. Doyle, "The complex structured singular value," *Automatica*, vol. 29, no. 1, pp. 71–109, 1993.

[25] G. Ferreres, *A Practical Approach to Robustness Analysis With Aeronautical Applications*. Berlin, Germany: Springer, 1999.

[26] A. Varga, G. Looye, D. Moormann, and G. Gräbel, "Automated generation of LFT-based parametric uncertainty descriptions from generic aircraft models," *Math. Comput. Model. Dyn. Syst.*, vol. 4, no. 4, pp. 249–274, 1998.

[27] A. Fabrizi, C. Roos, and J.-M. Biannic, "A detailed comparative analysis of μ lower bound algorithms," in *Proc. Eur. Control Conf.*, 2014, pp. 220–226.

[28] G. Balas, R. Chiang, A. Packard, and M. Safonov, "Robust control toolbox 3 user's guide," 2005.

[29] D. Piga, "Computation of the structured singular value via moment LMI relaxations," *IEEE Trans. Autom. Control*, vol. 61, no. 2, pp. 520–525, Feb. 2016.

[30] X. Chen and J. T. Wen, "Model reduction of multidimensional positive real systems," in *Proc. 1994 33rd IEEE Conf. Decis. Control*, Dec. 1994, pp. 3758–3763.

[31] M. Ferber, A. Korniienko, G. Scorletti, C. Vollaire, F. Morelzz, and L. Krhenbhl, "Systematic LFT derivation of uncertain electrical circuits for the worst-case tolerance analysis," *IEEE Trans. Electromagn. Compat.*, vol. 57, no. 5, pp. 937–946, Oct. 2015.
[32] J. C. Doyle, B. A. Francis, and A. Tannenbaum, *Feedback Control Theory*, vol. 1. New York, NY, USA: Macmillan, 1992.
[33] R. Castellanos, C. Juarez, J. Hernandez, and A. Messina, "Robustness analysis of large power systems with parametric uncertainties," in *Proc. IEEE Power Eng. Soc. Gen. Meeting*, 2006, pp. 1–8.
[34] M. Djukanovic, M. Khammash, and V. Vittal, "Application of structured singular value theory for robust stability and control analysis in multimachine power systems. II. Numerical simulations and results," *IEEE Trans. Power Syst.*, vol. 13, no. 4, pp. 1317–1322, Nov. 1998.
[35] R. Castellanos, A. Messina, and H. Sarmiento, "Robust stability analysis of large power systems using the structured singular value theory," *Int. J. Elect. Power Energy Syst.*, vol. 27, no. 5, pp. 389–397, 2005.
[36] M. Djukanovic, M. Khammash, and V. Vittal, "Application of the structured singular value theory for robust stability and control analysis in multimachine power systems. I. Framework development," *IEEE Trans. Power Syst.*, vol. 13, no. 4, pp. 1311–1316, Nov. 1998.
[37] S. Chen and O. P. Malik, "Power system stabilizer design using μ synthesis," *IEEE Trans. Energy Convers.*, vol. 10, no. 1, pp. 175–181, Mar. 1995.
[38] A. Haddadi, B. Boulet, A. Yazdani, and G. Joós, "A μ-based approach to small-signal stability analysis of an interconnected distributed energy resource unit and load," *IEEE Trans. Power Del.*, vol. 30, no. 4, pp. 1715–1726, Aug. 2015.
[39] D. -W. Gu, *Robust Control Design With MATLAB*, vol. 1. Berlin, Germany: Springer, 2005.
[40] S. Buso, "Design of a robust voltage controller for a buck-boost converter using μ synthesis," *IEEE Trans. Control Syst. Technol.*, vol. 7, no. 2, pp. 222–229, Mar. 1999.
[41] C. Zhang, J. Wang, S. Li, B. Wu, and C. Qian, "Robust control for PWM-based DC-DC buck power converters with uncertainty via sampled-data output feedback," *IEEE Trans. Power Electron.*, vol. 30, no. 1, pp. 504–515, Jan. 2015.
[42] J. A. Solsona, S. G. Jorge, and C. A. Busada, "Nonlinear control of a buck converter which feeds a constant power load," *IEEE Trans. Power Electron.*, vol. 30, no. 12, pp. 7193–7201, Dec. 2015.
[43] M. Fard and M. Aldeen, "Robust control design of a dc micro grid comprising photovoltaic and battery systems," in *Proc. 2016 IEEE PES Asia-Pac. Power Energy Eng. Conf.*, Oct. 2016, pp. 329–336.
[44] S. Sumsurooah, M. Odavic, S. Bozhko, and D. Boroyevich, "Stability and robustness analysis of a dc/dc power conversion system under operating conditions uncertainties," in *Proc. 41st Annu. Conf. IEEE Ind. Electron. Soc.*, Nov. 2015, pp. 003110–003115.
[45] S. Sumsurooah, M. Odavic, and S. Bozhko, "A modeling methodology for robust stability analysis of nonlinear electrical power systems under parameter uncertainties," *IEEE Trans. Ind. Appl.*, vol. 52, no. 5, pp. 4416–4425, Sep. 2016.
[46] S. Sumsurooah, M. Odavic, and S. Bozhko, "Development of LFT-based models for robust stability analysis of a generic electrical power system over all operating conditions," in *Proc. 2015 Int. Conf. Elect. Syst. Aircr. Railw. Ship Propulsion Road Veh.*, Mar. 2015, pp. 1–6.
[47] S. Sumsurooah, M. Odavic, and S. Bozhko, "μ approach to robust stability domains in the space of parametric uncertainties for a power system with ideal CPL," *IEEE Trans. Power Electron.*, vol. PP, no. 99, pp. 1–1, 2017,
[48] S. Sumsurooah, M. Odavic, and D. Boroyevich, "Modelling and robust stability analysis of uncertain systems," in *Proc. 2013 Grand Challenges Model. Simul. Conf.*, 2013, Paper 13.
[49] G. J. Balas, J. C. Doyle, K. Glover, A. Packard, and R. Smith, μ-Analysis and Synthesis Toolbox: For Use with MATLAB, 2001.
[50] R. W. Erickson and D. Maksimovic, *Fundamentals of Power Electronics*. Berlin, Germany: Springer, 2001.
[51] H. J. Zhang, "Modeling and loop compensation design of switching mode power supplies," *Linear Technology, Appl. Note 149*, 2015.
[52] A. A. Elbaset, "Small-signal MATLAB/Simulink model of dc-dc buck converter using state-space averaging method," in *Proc. 17th Int. Middle-East Power Syst. Conf.*, Mansoura University, Egypt, Dec. 15–17, 2015, pp. 1–8.
[53] D. Mattingly, "Designing stable compensation networks for single phase voltage mode buck regulators," Intersil, Milpitas, CA, USA, Tech. Rep. TB417.1, Dec. 2003.
[54] D. Meeks, "Loop stability analysis of voltage mode buck regulator with different output capacitor types—Continuous and discontinuous modes," , Texas Instruments, Dallas, TX, USA, App. Note SLVA301, 2008.

Sharmila Sumsurooah received the M.Sc. degree in electrical technology for renewable and sustainable energy systems in 2011, and the Ph.D. degree in robust stability analysis of power electronic systems in 2016, both from the University of Nottingham, Nottingham, U.K. Her Ph.D. degree was undertaken in collaboration with the Center for Power Electronics Systems, Virginia Tech, Blacksburg, VA, USA.

She was a visiting scholar in 2013 and 2014 at Virginia Tech. She is currently a Research Associate with the Power Electronics, Machines and Control Research Group of the University of Nottingham. Her research interests include robust stability analysis and optimization of electrical power systems in addition to modeling of multilevel converters.

Milijana Odavic (M'13) received the M.Sc. degree in electrical and electronic engineering from the University of Zagreb, Zagreb, Croatia, in 2004 and the Ph.D. degree in electrical engineering from the University of Nottingham, Nottingham, U.K., in 2008.

In 2013, she became a Lecturer in power electronics in the Electronic and Electrical Engineering Department, University of Sheffield, Sheffield, U.K. Prior to joining the University of Sheffield, she was a Research Fellow in the Power Electronics, Machines and Control Group, University of Nottingham and in the Department of Electric Machines, Drives and Automation, University of Zagreb. Her current research interests include design and control of power electronic converters for enhanced power quality and modeling, stability analysis, and control of power electronics dominated microgrids.

Serhiy Bozhko (M'96) received the M.Sc. and Ph.D. degrees in electromechanical systems from the National Technical University of Ukraine, Kyiv City, Ukraine, in 1987 and 1994, respectively.

Since 2000, he has been with the Power Electronics, Machines and Controls Research Group of the University of Nottingham, Nottingham, U.K. He is currently a Professor within this group and he leads several EU and industry funded projects in the area of aircraft electric power systems, including their architectures/topologies, control and stability, power management, as well as advanced modeling and simulations methods.

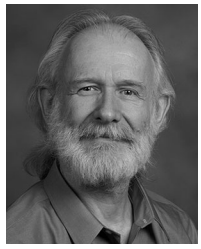

Dushan Boroyevich (F'06) received the Dipl.Ing. degree from the University of Belgrade, Belgrade, Serbia, in 1976 and the M.S. degree from the University of Novi Sad, Novi Sad, Serbia, in 1982, in what then used to be Yugoslavia. He also received the Ph.D. degree from Virginia Polytechnic Institute, Blacksburg, VA, USA, and State University (Virginia Tech), Blacksburg, VA, USA, in 1986.

From 1986 to 1990, he was an Assistant Professor and the Director of the Power and Industrial Electronics Research Program in the Institute for Power and Electronic Engineering, University of Novi Sad. He then joined the Bradley Department of Electrical and Computer Engineering, Virginia Tech, as an Associate Professor. He is currently a University Distinguished Professor and an Associate Vice-President for Research and Innovation in Energy Systems at Virginia Tech, and the Director of the Center for Power Electronics Systems. He has advised more than 40 Ph.D. and 40 M.S. students to graduation and has coauthored with them over 700 papers. He has led numerous research projects in the areas of multiphase power conversion, electronic power distribution systems, modeling and control, and multidisciplinary design optimization.

Dr. Boroyevich was the President of the IEEE Power Electronics Society (PELS) for 2011–2012. He received the numerous awards, including the IEEE William E. Newell Power Electronics Technical Field Award, the IEEE PELS Harry A. Owen Distinguished Service Award, the European Power Electronics Association Outstanding Achievement Award, and the Award for Outstanding Achievements and Service to Profession by the European Power Electronics and Motion Control Council. He is an Honorary Professor at the Xi'an Jiaotong University, Xi'an, China, and the K. T. Li Chair Professor at the National Cheng Kung University, Tainan, Taiwan. He was elected to the US National Academy of Engineering in 2014 for advancements in control, modeling, and design of electronic power conversion for electric energy and transportation.